Design of Microfabricated Rectangular Coaxial Lines and Components for mm-Wave Applications

Dejan S. Filipović, Zoya B. Popović, Milan V. Lukić and Kenneth Vanhille

Abstract— **Miniature 310μm tall copper-air rectangular coaxial lines (RCL) with the inner conductor supported by periodic dielectric straps are demonstrated in this paper. The measured line loss is about 0.2dB/cm at 26GHz, while the isolation between two parallel lines with a center-to-center separation of 700μm is better than 60dB. Several quasi-planar components are designed and fabricated on the same wafer, and presented here are a branch line hybrid, a cavity resonator, and a cavity-backed patch antenna. The through and coupled port transmissions for the hybrid at 26GHz are 3.25dB and 3.35dB, respectively, with an output phase misbalance below 0.2°. The fabricated resonator has an unloaded Q-factor of 530 at 26GHz. The measured bandwidth of the antenna is 4.5% near 35GHz. The coaxial lines and other passive components are built with a new sequential micromachining process capable of utilizing copper as structural material, and polymer for the support of the inner conductor. A detailed description of the analysis, design, fabrication and performance is provided.**

Keywords—**Coaxial line, Computer aided design, Branch line hybrid, Transmission Line Resonator.**

I. INTRODUCTION

Recent advances in the micro-electromechanical systems (MEMS) fabrication techniques [1-3], including surface and bulk micromachining, provide ample opportunities for the use of a small rectangular coaxial line (RCL), also known as recta-coax. Highly integrated designs and assembly of non-dispersive, high isolation lines, components, and micro-electromagnetic radio frequency systems (MERFS) sub-systems operating in the millimeter and sub-millimeter bands are becoming feasible. A number of novel recta-coax structures with heights from 50μm to 400μm have already been reported. For instance, air-filled RCLs built using different variations of surface micromachining are demonstrated in [4]. Very promising results with somewhat higher losses than the theoretical predictions are obtained. Branch line hybrids [5, 6] and filters [7], are recent examples of miniature RCL based components designed to operate in frequency ranges up to V-band. These lines and components are typically analyzed using 3D finite element based solvers.

In this paper, we discuss modeling of miniature 310μm tall inhomogeneous copper recta-coax lines (see Fig. 1) and components as well as novel sequential microfabrication process [8] that enables their practical realization. The performances of the basic transmission lines, branch line hybrid, single post cavity resonator and antenna are obtained computationally and experimentally. The paper is organized as follows: a discussion on modeling and design is given in Section II, followed by the description of the fabrication process in Section III. Measured performances of the RCL, hybrid, resonator and antenna are presented in Section IV.

The authors are with the Department of Electrical and Computer Engineering, University of Colorado, Boulder, CO 80309-0425 USA phone: 303-735-6319; fax: 303-492-2758;
(e-mail: {dejan,zoya,milan.lukic,vanhille}@colorado.edu).

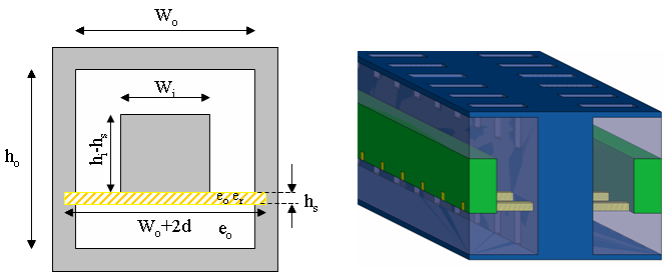

Fig. 1. Sketches of a rectangular μ-coaxial line. Shown on the left is a 2D cross section, while the relative positioning of the dielectric support and the release holes are depicted on the right. The line parameters are: $\{W_o, h_o, W_i, h_i, h_s, L_h, w_h\} = \{0.25, 0.25, 0.1, 0.1, 0.015, 0.2, 0.1\}$ mm; $\varepsilon_r=3.7$, $\tan\delta=0.05$. The periodicity and the width of the support straps are 0.7mm and 0.1mm, respectively.

II. ANALYSIS AND DESIGN

A. Challenges

Analysis of miniature rectangular coaxial lines and components is a challenging task. The issues can be argued from geometrical and computational perspectives (see Fig. 2). The multi-layered configuration, a combination of small and large structural features, homogeneous and inhomogeneous cross-sections, sharp corners and roughness, the misalignment of structural layers, the need for release holes, etc. are just a few examples of geometrical concerns that must be considered. The analysis method must be capable of easy 2D and 3D formulation and solution of closed domain structures. However, the effects of the release holes, particularly the radiation through them must be also modeled. As the computational domain contains both small and large features, and materials of different dielectric constant and high/low aspect ratio, with a combination of rough and smooth surfaces, there are severe restrictions on the choice of modeling tools. Finally, a capability for the easy definition of excitations, boundary conditions, material parameters, and extraction of performance parameters must be also accounted for.

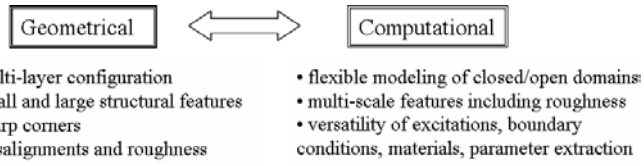

Fig. 2 Overview of the geometrical and computational challenges that must be accounted for.

B. Modeling Approach and Validation

To address all the above issues, a modeling approach combining robust 2D and 3D eigenanalysis (EA) and driven finite element method (FEM) formulations within Ansoft's High Frequency Structure Simulator (HFSS) and quasi-static (QS) single and double connected Schwartz-Christoffel conformal mapping (SCCM) [9] are utilized. The applicability of these methods along with a numerical validation are demonstrated in Fig. 3.

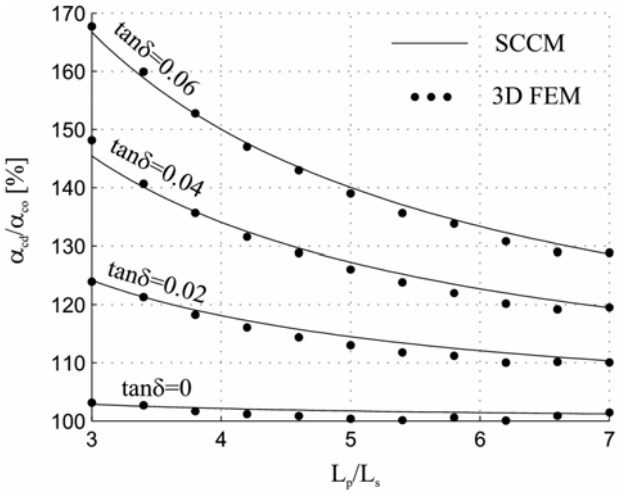

Fig. 3. Computational validation and design results for an inhomogeneous recta-coax line with varying periodicity ratio. Compared are the full-wave simulations using HFSS and the combined circuit/SCCM model. A dielectric constant of 4.2 is assumed for the losses depicted in the figure.

C. RCL and Component Design Studies

The variation of the air-coax RCL's attenuation, characteristic impedance and the cut-off frequency for the first higher order mode are depicted in Fig. 4. The attenuation constant and impedance are computed with the SCCM and Wheeler's incremental inductance rule, while the 2D eigen-analysis within HFSS was utilized for the cut-off frequency [10]. As seen, though a wider range of impedances can be obtained, the variations of the attenuation and cut-off frequency around the nominal values are not that significant.

The surface roughness can be a significant contributor to the overall loss of the RCLs. However, the detailed modeling and measurements have not been conducted so far. Additionally, commercial solvers and textbooks utilize and argue the use of different formulas, whose origins typically come from the investigation of microstrip lines. Increased electrical length of the lines, albeit relatively small, can be very significant in many applications with very long lines, including the beamforming networks for phased arrays. Sketches of two investigated profiles are shown in Fig. 5. It is found that the appropriate formula for computing the excess attenuation due to the rough vertical walls of a RCL with grooves transversal to the current flow is:

$$\alpha_{c'} = \alpha_c \left(1 + \frac{A_1}{\pi} \tan^{-1} \left(A_2 \left(\frac{\Delta}{\delta_s} \right)^2 \right) \right)$$

with A1, A2 = (0.69, 2.1) and (0.75, 2.2) for homogeneous and inhomogeneous lines, respectively [12]. Δ is the RMS roughness while δs denotes the skin depth value.

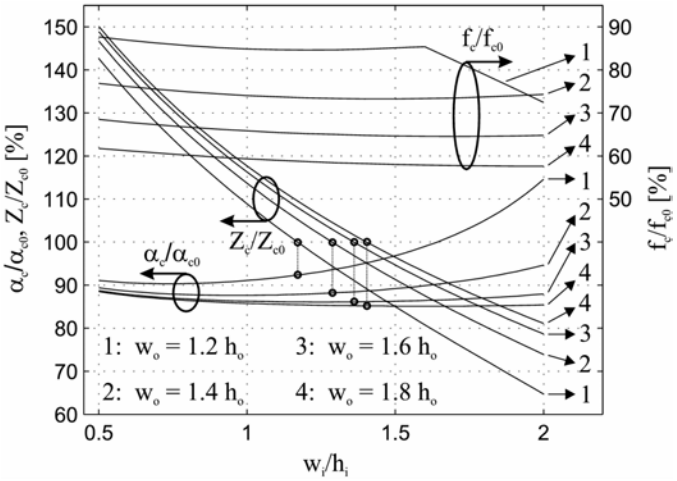

Fig.4. Normalized attenuation (α_{c0}=0.161dB/cm), characteristic impedance (Z_{c0}=50Ω) and cut-off frequency (f_{c0}=467.5GHz) for RCL versus inner conductor width for different outer conductor widths. The heights of inner and outer conductors are kept constant.

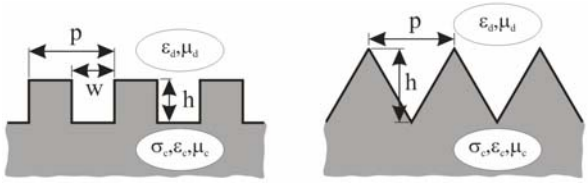

Fig. 5. Various geometrical models utilized for the analysis of surface roughness effects on the RCL performance. Rectangular (left) and triangular (right) grooves are shown.

The initial studies of the 90° hybrids are conducted using a circuit simulator with ideal transmission lines and junctions. The sensitivity of the output amplitude imbalance to the parameters of the hybrid is studied. One such study is given in Fig. 6, which examines the effect of changing the characteristic impedance of the Port 1-2 and Port 3-4 branches of the hybrid (where port 1 is the input, port 2 is the output, port 3 is the coupled port, and port 4 is the isolated port.). It is seen that if the characteristic impedance of those branches is off by even 1Ω compared to the ideal (an error which translates into a couple of microns of width for a 150μm-wide inner conductor), the amplitude misbalance at the output port

can be 0.25dB. Eventually, the devices are modeled using HFSS, including the losses and effects from the substrate, the release holes, radiation, and conductor losses. Because the cut-off frequency of the next higher-order mode (467.5GHz) is so much greater than the operating frequency, the parasitic reactances associated with the junctions are quite small. Therefore, the circuit simulation using lossy transmission lines with ideal junction models gives similar results to the full-wave methods.

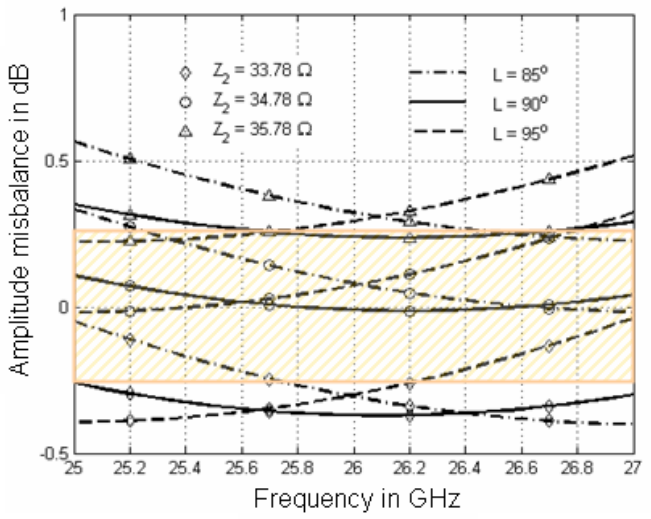

Fig. 6. Spread of the predicted amplitude misbalance for 9 different hybrids with parameters depicted in the inset.

Several cavity resonators are developed using the process described here [12]. The analytical formulation for a rectangular waveguide cavity resonator is used as a starting point for the designs [13]. Fig. 7 shows computed values for the quality factor of the resonator for different ratios of the side lengths of the cavity resonator for the TE101 mode. It is found that a resonator size of 8.159mm by 8.159mm by 250μm gives the resonance at 26.0 GHz with an ideal unloaded Q of 574. One sees that although the maximum Q is achieved when the dimensions of the two sides are equal, a ratio of 3/1 between the two sides does not decrease the Q of the resonator more than 3%. In high density circuits, this may give the designer added flexibility in designing the resonators if a long and narrow resonator footprint may prove better in some situations than a square one. The full resonator, including release holes, the launch, the substrate, the support post for mechanical stability, and the radiation is modeled using HFSS. Half symmetry can be utilized to reduce the size of the computational domain. The resonant frequency and unloaded Q can be found using either EA or a driven formulation, however the frequency response and the loaded Q are best found using a driven method.

A patch antenna with the pulled-up side cavity walls compatible with the developed process is designed to operate at around 37GHz. The patch is supported by three posts placed in the antenna's physical center (corresponds to the minimum electric field for the fundamental TE010 mode), and the 250μm tall cavity is air-filled. The release holes on the top layer are 200×200μm2, while those in the side walls are 200×75μm2. Radiation patterns in E- and H-planes are shown in Fig. 8, and as seen similar 3dB beamwidths are obtained. Computed gain is about 8.5dBi, and the resonant resistance is very high around 320Ω, however, using standard techniques including the slits around the feed or offset feed could be utilized to reduce this value down to 50Ω.

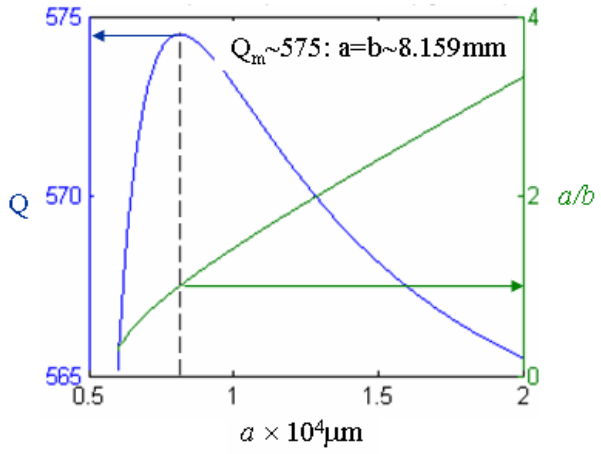

Fig. 7. Analytical values for the unloaded Q of a TE_{101} mode of a 250μm tall copper cavity resonator as a function of the resonator sides *a, b*. As seen, the maximum value is obtained for the square cavity (~574) with the interior edge length of *a*=*b*=0.8159cm.

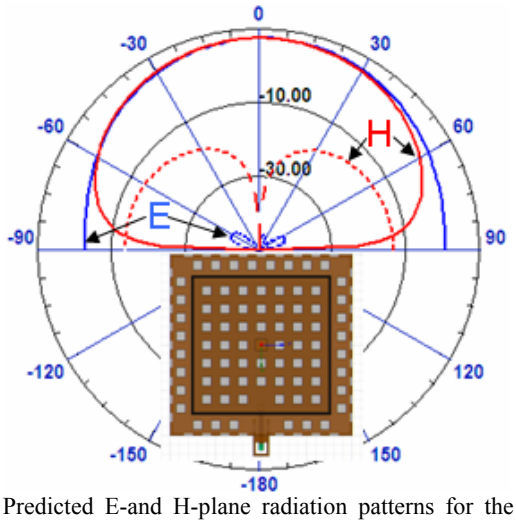

Fig. 8. Predicted E-and H-plane radiation patterns for the cavity-backed patch at the resonance.

III. FABRICATION

Recta-coax lines and components are fabricated using a new sequential microfabrication process described in [8], and schematically represented in Fig. 9. Similar to the surface micromachining technique, the recta-coax structures are built up layer by layer by depositing a uniform copper stratum (layer 1), and sequence of strata comprised of photo-resist and copper (layers 2, 4, and 5). Polymer support is a part of the 3rd layer. The heights of layers 1-5 are {10, 75, 100, 75, 50} μm, respectively. Once the structure is built, the resist is

drained through the holes in the top and side walls. These openings are referred to as release holes. A scanning electron microscope (SEM) photo of a part of the fabricated wafer is shown in Fig. 10. Shown in the picture are different recta-coax lines, calibration structures, test sets for isolation, and several different cavity resonators. The components are built on a 15cm diameter and 1mm thick high resistivity Si wafer, however, other substrates may also be used. Shown in Fig. 11 are photos of different views of the MERFS launches.

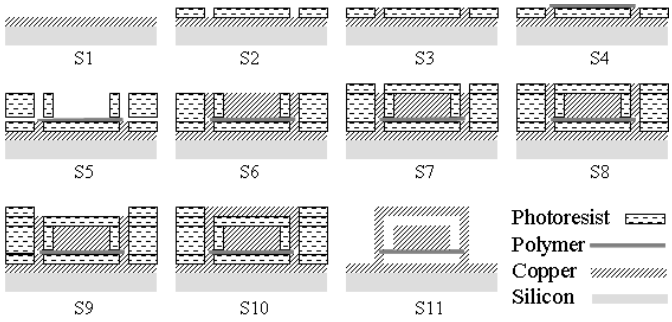

Fig. 9. Simplified sketch of the steps undertaken in the sequential building process (left to right, top to bottom). The end result is a non-uniform air-polymer RCL comprised of 5 strata.

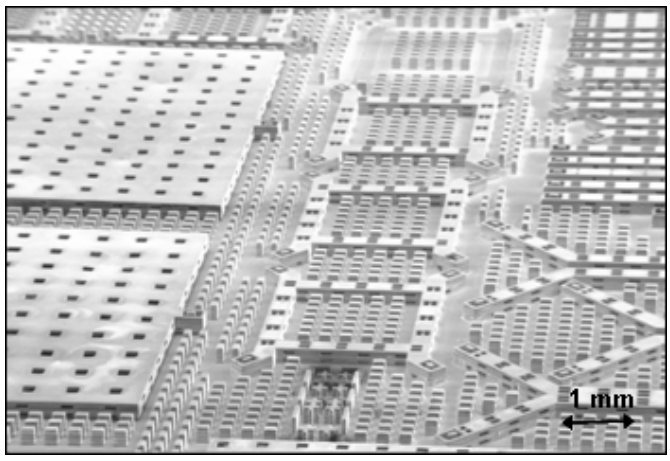

Fig. 10. SEM photograph of a portion of the fabricated wafer showing a number of hybrids and coaxial lines with various separation distances, as well as portions of cavity resonators (larger objects visable on the left of the photo). The 250×300μm launches into the lines are visible as rectangular coaxial openings at the end of each line/component. The holes in the top and side walls are used for releasing the photoresist in the last fabrication step, thus leaving the interior of the line and structures air-filled (except for the dielectric support)

IV. Measured Recta-Coax Structures

Several 310μm tall rectangular and square 50Ω coaxial lines are designed and fabricated. They are composed of five structural layers forming the inner and outer conductors. The inner conductor is supported by periodically (700μm) spaced 18μm tall and 200μm wide dielectric supports (εr=3.7, tanδ=0.05). The support straps are firmly held between layers 2 and 3. As shown in Fig. 1, the release holes in side (100μm×75μm) and top walls (200μm×100μm) are placed in the region between the straps. HFSS and SCCM are used to fully characterize the performance of the line. Electrical effects of potential fabrication issues such as strap parameters including the protrusion into the vertical walls, offset layers, under/over etching, surface roughness, are given in [10,11]. It is found that the performance of the line built within the limits of fabrication tolerances is almost the same as the performance of a perfectly constructed structure.

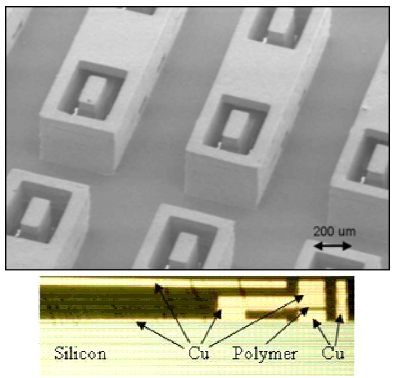

Fig. 11. SEMs of the recta-coax feed sections. Shown are several test structures for de-embedding and calibration (top) and a cross-section of the launch from on of fabricated resonators (bottom).

Several passive components, including branch-line hybrids, cavity backed patch antennas, as well as cavity and transmission line resonators are fabricated on the same wafer. Here we show results for a hybrid and a transmission line resonator.

A. Recta-Coax Line

Measured attenuation of several 50Ω lines is shown in Fig. 12, having loss of 0.22dB/cm at 26GHz. The measurements are calibrated using external short-open-load-thru (SOLT) calibration. Shown in the same figure is the cross section of the characterized structures.

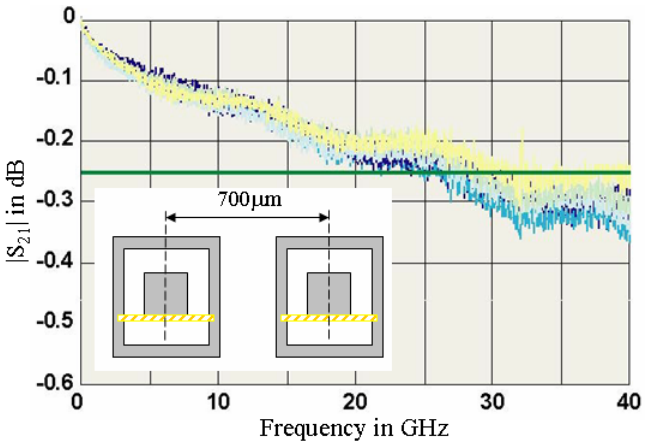

Fig. 12. Measured insertion loss of 1cm long lines separated by 700μm. This test set-up is different than the one shown as the inset in the Fig. 13.

Given in Fig. 13 is the measured isolation between two lines with center-to-center separation of 700μm. The computational model is depicted in the same figure. It was determined that the main coupling mechanism of a non-metalized layer 1 structure is through the launch opening, and that the special care must be exercised for the mitigation thereof. Specifically, the coupling can increase for almost 20dB if layer 1 is not metalized. While complete layer-1 metal deposition can produce damaging stress levels on the wafer, a careful design can mitigate this risk while significantly reducing cross-talk between neighboring lines. Measured isolations and standard deviations (σ) for several test structures are given in Table I.

TABLE I. MEASURED ISOLATION FOR TWO ADJACENT PARALLEL LINES SEPARATED BY 700μM.

F [GHz]	$\|S_{31}\|$ [dB]	$\sigma(\|S_{31}\|)$	$\|S_{41}\|$ [dB]	$\sigma(\|S_{41}\|)$
24	- 63.0	0.83	- 65.2	0.53
26	- 62.5	0.89	- 62.5	1.09
28	- 62.7	0.57	- 60.9	0.80

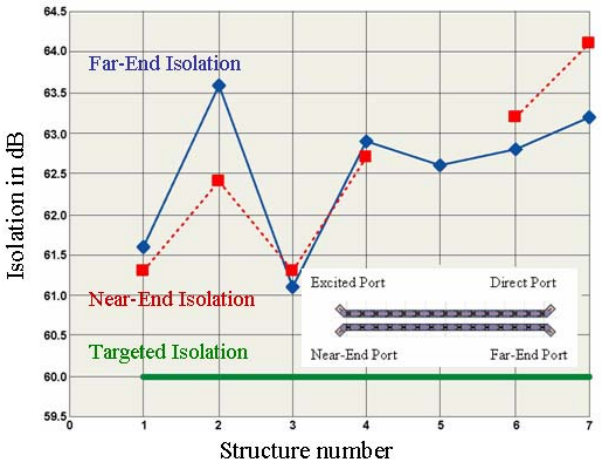

Fig. 13. Measured isolation for the two lines separated center-to-center by 700μm.

B. *Branch-Line Hybrid*

μ-coaxial branch-line hybrids have been demonstrated using different fabrication technique with nickel as the structural metal instead of copper and with short metallic posts supporting the inner conductor [6,7]. Here, we followed a standard 90° hybrid design procedure [13]. Special care was exercised in studying the effects of the release holes and dielectric support. It was found that they have a small effect on amplitude and phase balance. Measured S-parameters are shown in Fig. 14. At the design frequency of 26GHz, measured amplitude misbalance is 0.1dB (S31=-3.35dB, S21=-3.25dB). The isolation is around 19dB and the return loss is about 17dB. None of the T-junction compensation techniques was implemented.

C. *Resonator*

Five different cavity resonators are designed, built and characterized (four realizations are given in [12]). The insertion loss and the sketch of a single post resonator protruding to the silicon wafer are shown in Fig. 15. The procedure for extracting the unloaded Q is given as inset in the same figure. The fabricated resonator resonates at 26.22GHz with the unloaded Q factor of 490. To reduce the losses due to the fringing fields in the wafer, a high resistivity Si wafer was utilized in fabrication.

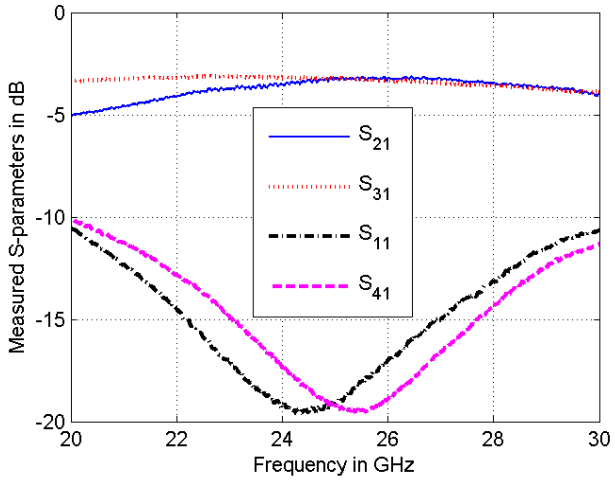

Fig. 14. Measured S parameters for the hybrid. The input, through, coupled and isolated ports are denoted as 1, 2, 3 and 4, respectively.

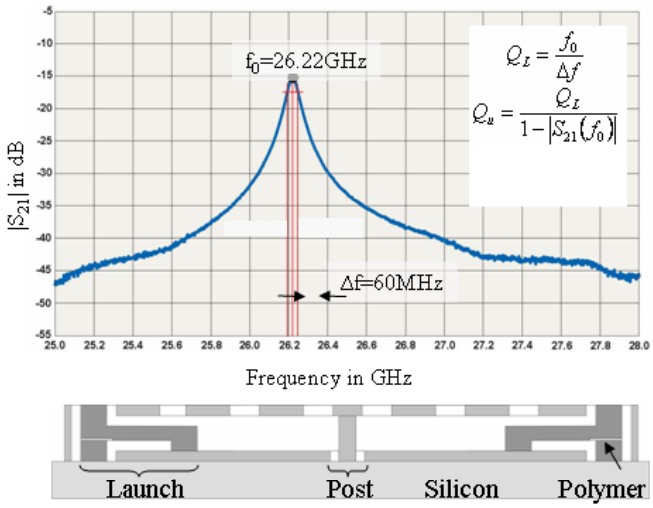

Fig. 15. Measured insertion loss of the 2-port resonator (top) with the metallic post to silicon in the center (bottom). Shown in the inset is the set of formulae used to obtain value for the unloaded Q-factor.

D. *Antenna*

A MERFS compatible resonant patch with pulled-up cavity walls and its measured return loss are shown in Fig. 16. The resonant impedance was high as expected for this structure.

Standard procedures are available for mitigating this effect, including the use of tuning slits (effectively making the E-shaped patch), and capacitive loading within the launch. Interestingly, post needed to hold the patch, along with the pulled up walls contributes to the second resonance with the monopole like pattern. Note that the effect of the release holes on the performance of this antenna is minimal.

V. SUMMARY

The analysis and design of μ-coaxial lines and components compatible with the sequential planarized photolithographic like process are presented in this paper. Very low loss of 0.22dB/cm at 26GHz and high isolation better than 60dB for 700μm center to center separated lines are measured. The amplitude and phase misbalances below 0.1dB and 0.2° respectively are also obtained with the branch-line coupler. High Q-factor resonator and MERFS compatible patch radiator are other components designed to further demonstrate the capabilities of the developed microfabrication process. Finally, excellent agreement between modeled and measured results is demonstrated.

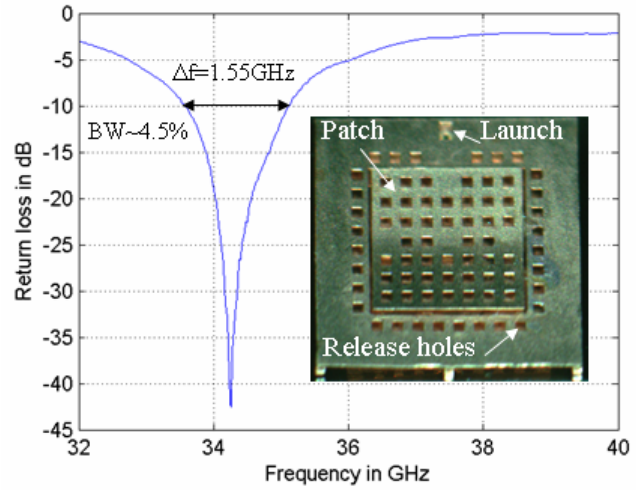

Fig. 16. Measured return loss at the launch with respect to the resonant resistance of 360Ω. As seen, the overall 10dB return loss bandwidth of 4.5% is achieved. Notice that the further optimization and design are needed for matching to 50Ω.

ACKNOWLEDGMENT

This work was supported by the DARPA-MTO under the 3D Micro-Electromagnetics Radio Frequency Systems (3d MERFS) program. Authors would like to acknowledge Yuya Saito, Michael Buck, Dr. Sebastien Rondineau from University of Colorado, Dan Fontaine and Gil Potvin from BAE Systems, Chris Nichols from Rohm and Hass, and W. Wilkins from Mayo Foundation for their contributions to this paper.

REFERENCES

[1] R. Chen, "Micro-fabrication techniques," *Wireless Design and Development*, pp. 16-20, Dec. 2004.

[2] J.-B. Yoon, B.-I. Kim, Y.-S. Choi, and E. Yoon, "3-D construction of monolithic passive components for RF and microwave ICs using thick-metal surface micromachining technology," *IEEE Trans. Microwave Theory Tech.*, vol. 51, no. 1, pp. 279-288, Jan. 2003.

[3] I. Jeong, S.-H. Go, J.-S. Lee, and C.-M. Nam, "High-performance air-gap transmission lines and inductors for mm-wave applications," *IEEE Trans. Microwave Theory Tech.*, vol. 50, no.12, pp. 2850-2855, Dec. 2002.

[4] E. Brown, A. Cohn, C. Bang, M. Lockard, B. Byrne, N. Vandlli, D. McPherson and G. Zhang, "Characteristics of microfabricated rectangular coax in Ka band," *Microwave and Optical Tech. Lett.*, vol. 40, no. 5, pp. 365-368, March 2004.

[5] J. Reid and R. Webster, "A 60GHz branch line coupler fabricated using integrated rectangular coaxial lines," *Proc. IEEE MTT-S Int. Microwave Symp. Digest*, Fort Worth, TX, June, 2004, pp. 441-444.

[6] R. Chen, E. Brown and R. Singh, "A compact 30GHz low loss balanced hybrid coupler fabricated using micromachined integrated coax," *Proc. IEEE Radio Wireless Conf.*, pp. 227-230, Sept. 2004.

[7] J. Reid and R. Webster, "A compact integrated V-band bandpass filter," Proc. 2004 IEEE AP-S Int. Symp., Monteray, CA, July 2004, pp. 990-993.

[8] D. Sherrer and J. Fisher, "Coaxial waveguide microstructures and the method of formation thereof," U.S. Patent Application Publication No. US 2004/0 263 290A1, Dec. 30, 2004.

[9] T. Driscoll and L. Trefethen, *Schwarz-Christoffel Mapping*, Cambridge Univ. Press, 2002.

[10] M. Lukic, S. Rondineau, Z. Popovic and D. Filipovic, "Modeling of realistic μ-coaxial lines," *IEEE Trans. Microave. Theory Tech.*, vol. 54, no. 5, pp. 2068-2076, May 2006.

[11] K. Vanhille, D. Fontaine, C. Nichols, D. Filipovic, and Z. Popovic, "Quasi-planar high-Q millimeter-wave resonators," *IEEE Trans. Microave. Theory Tech.*, vol. 54, no. 6, pp. 2439-2446, June 2006.

[12] M. Lukic and D. S. Filipovic, "Modeling of surface roughness effects on the performance of rectangular μ-coaxial lines," *ACES Conference*, pp. 620-625, March 2006.

[13] D. Pozar, *Microwave Engineering*, 3rd Edition, Wiley, 2004.